Electronic Supplementary Material (ESI) for Energy & Environmental Science.

Supporting Information

Twinborn TiO_2-TiN heterostructures enabling a smooth trapping-diffusion-conversion of polysulfides towards ultralong life lithium-sulfur batteries

Tianhong Zhou [a,b], Wei Lv [a,*], Jia Li [a], Guangmin Zhou [c], Yan Zhao [a,b], Shaoxun Fan [a,b], Bilu Liu [d], Baohua Li [a,*], Feiyu Kang [a,b,d] and Quan-Hong Yang [a, d, e,*]

[a] Shenzhen Key Laboratory for Graphene-based Materials and Engineering Laboratory for Functionalized Carbon Materials, Graduate School at Shenzhen, Tsinghua University, Shenzhen 518055, China

[b] Laboratory of Advanced Materials, School of Materials Science and Engineering, Tsinghua University, Beijing 100084, China

[c] Shenyang National Laboratory for Materials Science, Institute of Metal Research, Chinese Academy of Science, Shenyang 110016, China

[d] Tsinghua-Berkeley Shenzhen Institute (TBSI), Tsinghua University, Shenzhen 518055, China

[e] School of Chemical Engineering and Technology, Tianjin University, Tianjin 300072, China

* Corresponding author. Email: lv.wei@sz.tsinghua.edu.cn (W.L.);

libh@mail.sz.tsinghua.edu.cn (B.H.L);

yang.quanhong@sz.tsinghau.edu.cn or qhyangcn@tju.edu.cn (Q.H.Y.).

Supporting Information

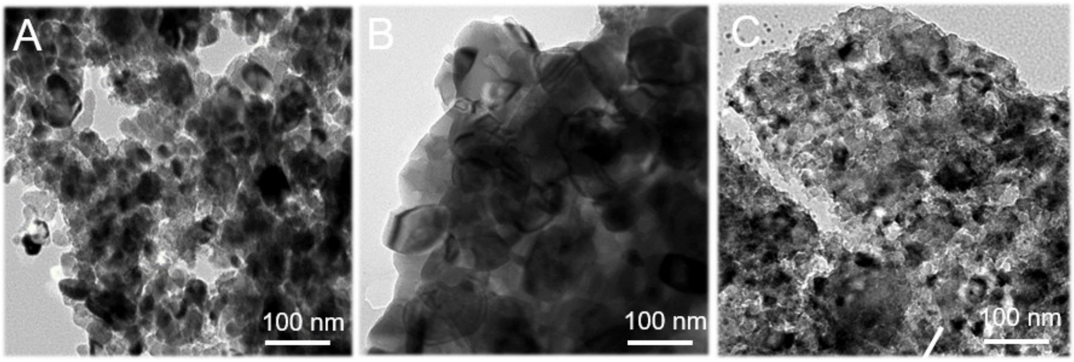

Fig. S1. Low magnification TEM images. (a) single phase TiN, (b) rutile TiO_2, and (c) TiO_2-TiN heterostructure.

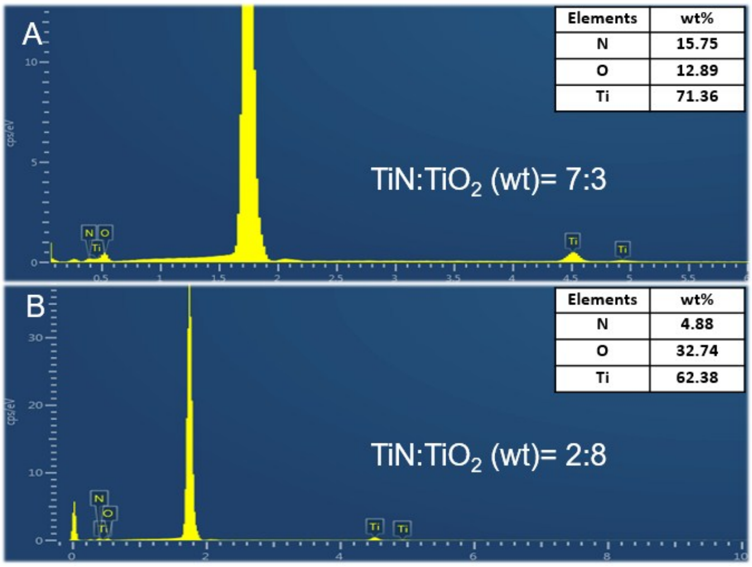

Fig. S2. Energy dispersive X-ray spectroscopy (EDS). (a) 2TiN: $8TiO_2$, (b) 7TiN: $3TiO_2$.

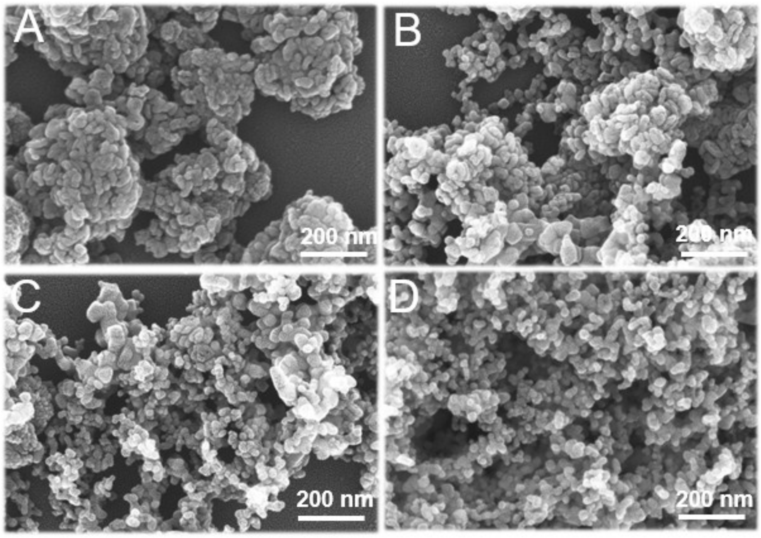

Fig. S3. SEM images. (a) TiO_2, (b) 2TiN: $8TiO_2$, (c) 7TiN: $3TiO_2$ and (d) TiN.

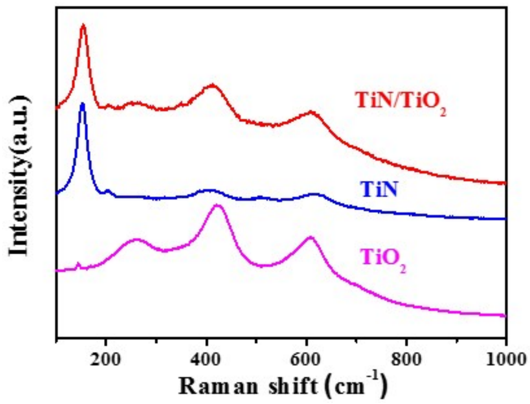

Fig. S4. Phase characterization. Raman spectroscopy for the as-synthesized single phase TiN, rutile TiO_2, and TiO_2-TiN heterostructures.

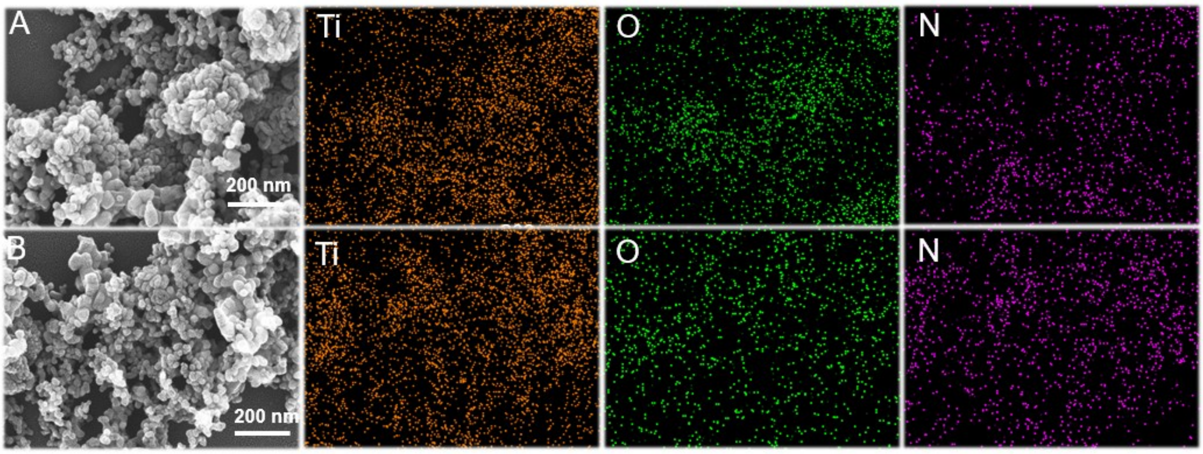

Fig. S5. Element mappings (titanium, oxygen, nitrogen). (a) 2TiN: $8TiO_2$, (b) 7TiN: $3TiO_2$.

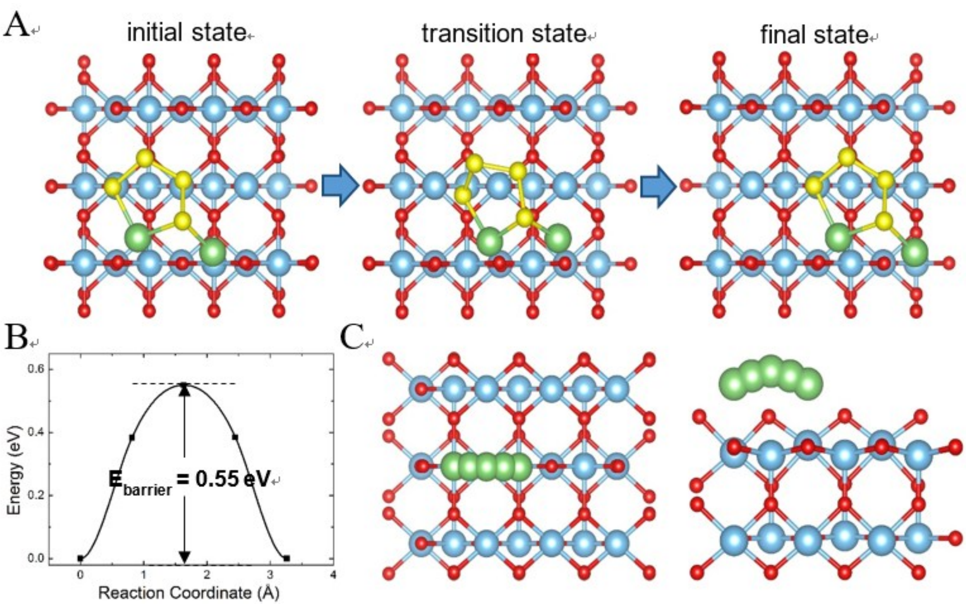

Fig. S6. The geometrical configurations of Li_2S_4 and lithium diffusion. (a) Initial state, transition state, and final state of Li_2S_4 migration along the [001] direction on the rutile TiO_2 (110) surface; (b) Energy profile for lithium migration along [001] direction on the rutile TiO_2 (110) surface; (c) Top and side views of minimum energy path for lithium migration along [001] direction on the rutile TiO_2 (110) surface.

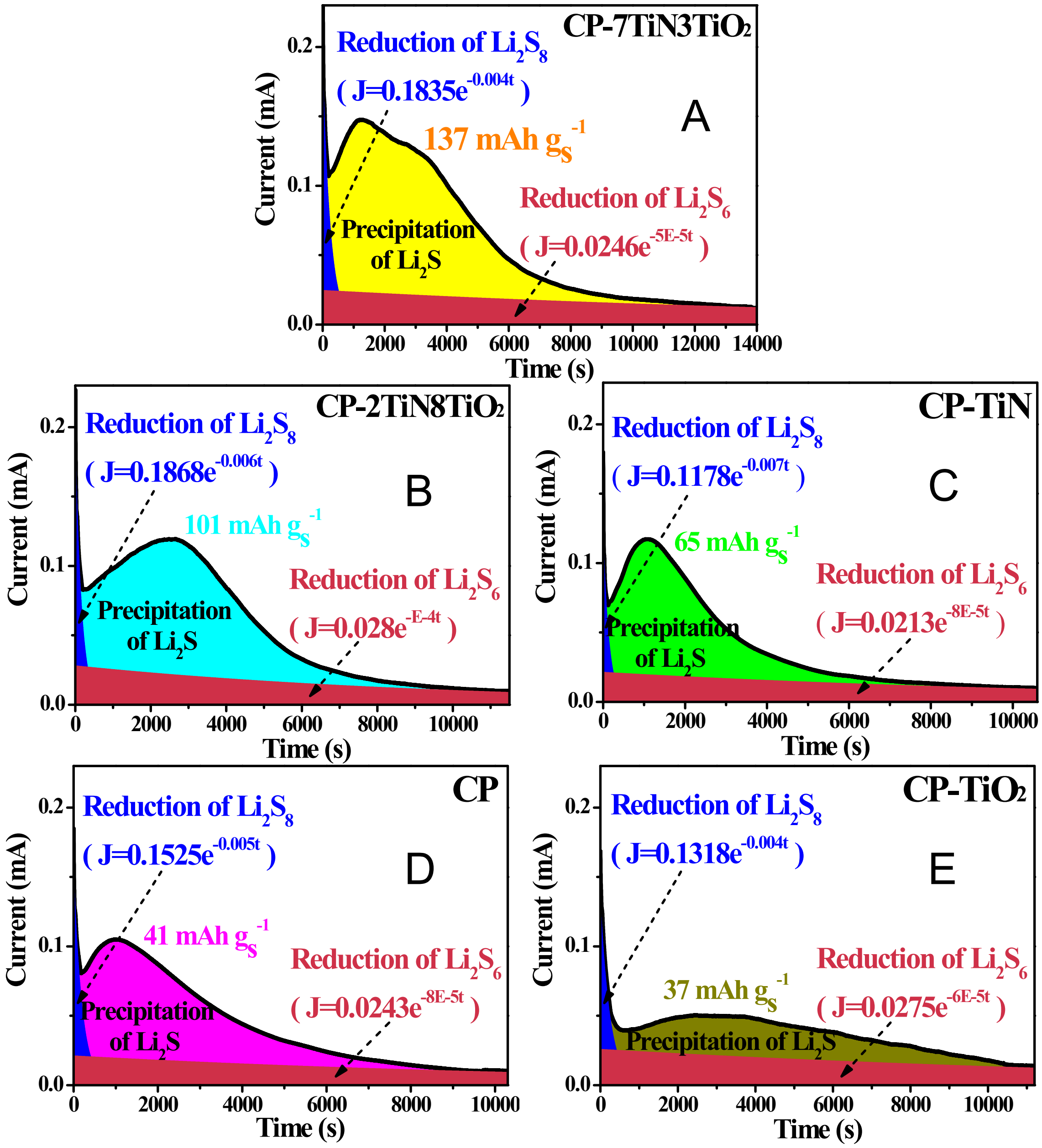

Fig. S7. Fitting of current vs. time curve on different surfaces. (a) CP-7TiN:3TiO_2, (b) CP-2TiN: 8TiO_2, (c) CP-TiN, (d) CP, (e) CP-TiO_2. The cells were discharged galvanostatically at 0.112 mA to 2.06 V and kept potentiostatically at 2.05 V until the current was below 10^{-5} A. The whole process of Li_2S nucleation/growth lasted for 11,000 s approximately. The nucleation/growth rate of lithium sulfide were mathematically evaluated based on the whole charge according to Faraday's law.

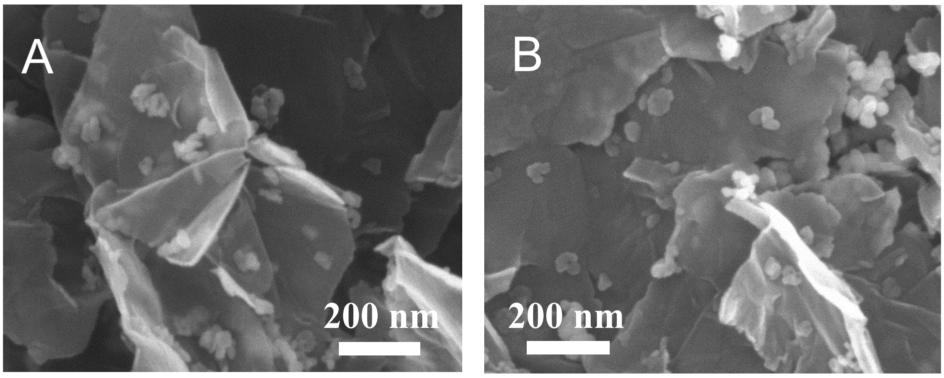

Fig. S8. The structure of TiO_2-TiN-G. (a) 7TiN: 3TiO_2-G, (b) 2TiN: 8TiO_2-G.

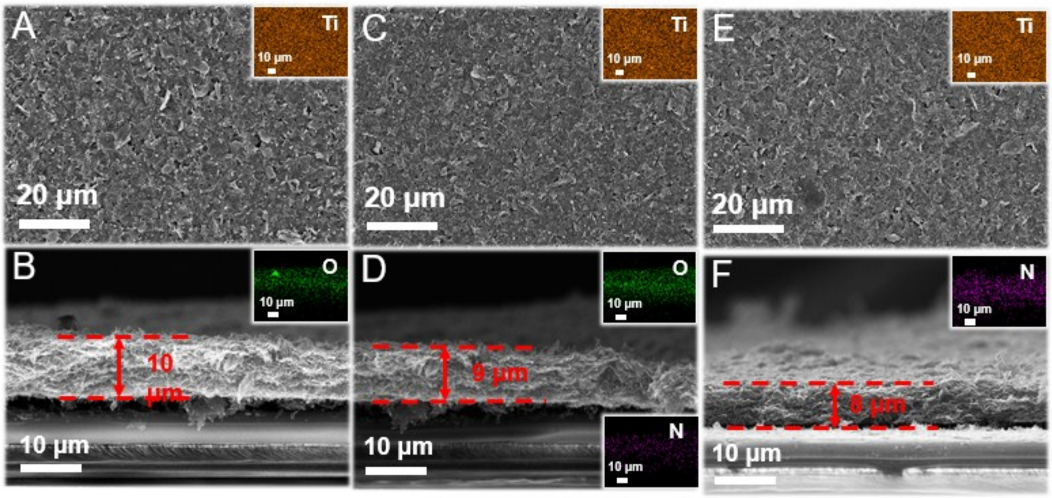

Fig. S9. SEM images of typical top-view and cross-sectional images of the coatings. (a and b) TiO_2-G; (c and d) 2TiN: 8TiO_2-G; (e and f) TiN-G coating layers, the insets are elemental distribution maps.

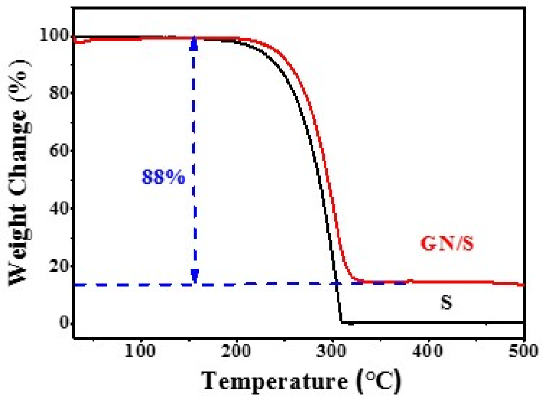

Fig. S10. The loading of sulfur in active materials. Thermogravimetric analysis (TGA) for the graphene-sulfur hybrid and pure sulfur.

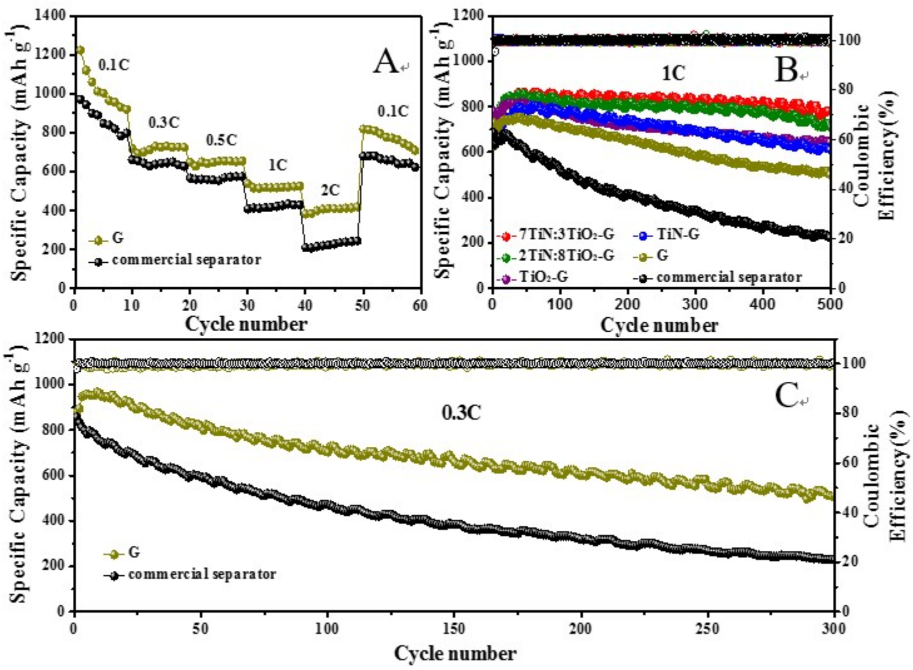

Fig. S11. Electrochemical performances of cells with graphene-only coated separators (G) and commercial separator. (a) rate performance at different current densities, (b) cycling stability of cells with different as-synthesized TiO_2-TiN coating layer as well as the control samples (7TiN: $3TiO_2$-G, 2TiN: $8TiO_2$-G, TiO_2-G, TiN-G, G, commercial separator) at 1 C for 500 cycles, (c) cycling stability at 0.3 C for 300 cycles.

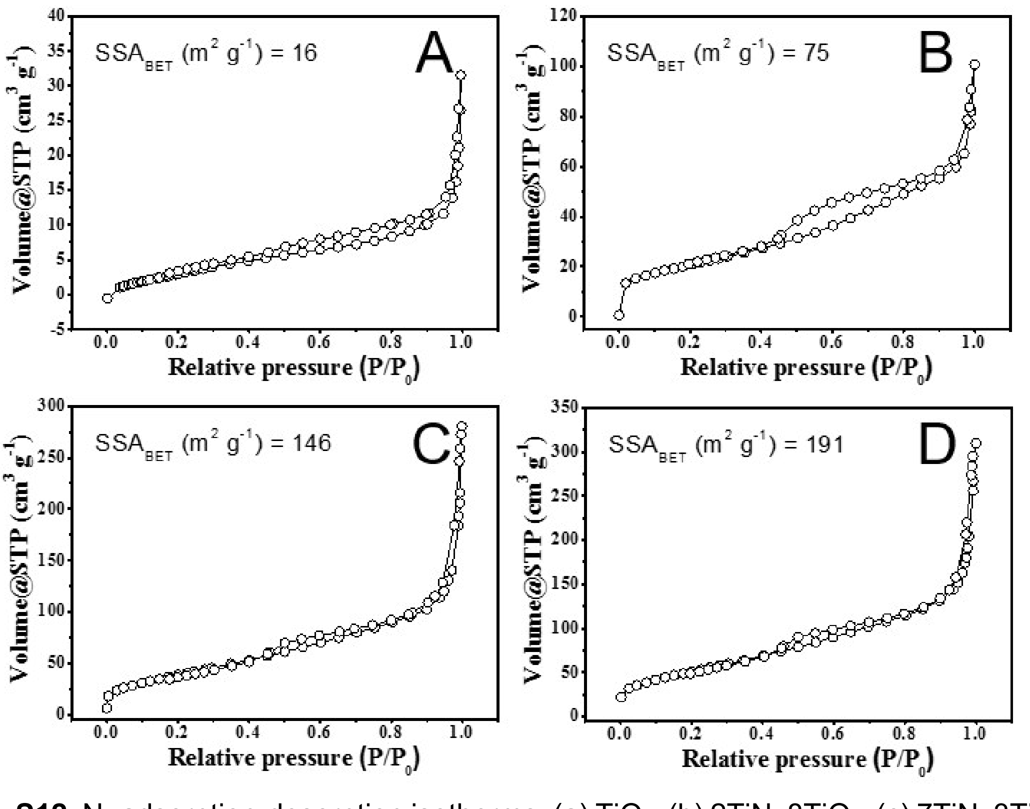

Fig. S12. N_2 adsorption-desorption isotherms. (a) TiO_2, (b) 2TiN: $8TiO_2$, (c) 7TiN: $3TiO_2$ and (d) TiN.

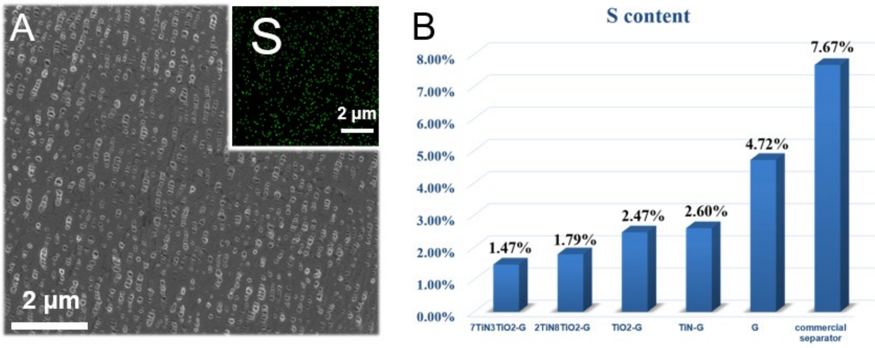

Fig. S13. Sulfur content after cycling. (a) SEM image of the separator with 7TiN: 3TiO_2-G coating layer (close to the lithium anode) after 500 cycles at 1 C, the inset is its elemental map for sulfur. (b) Sulfur content from EDS of the separators with different as-synthesized TiO_2-TiN coating layers as well as the control samples (7TiN: 3TiO_2-G, 2TiN: 8TiO_2-G, TiO_2-G, TiN-G, G, commercial separator) after cycling.

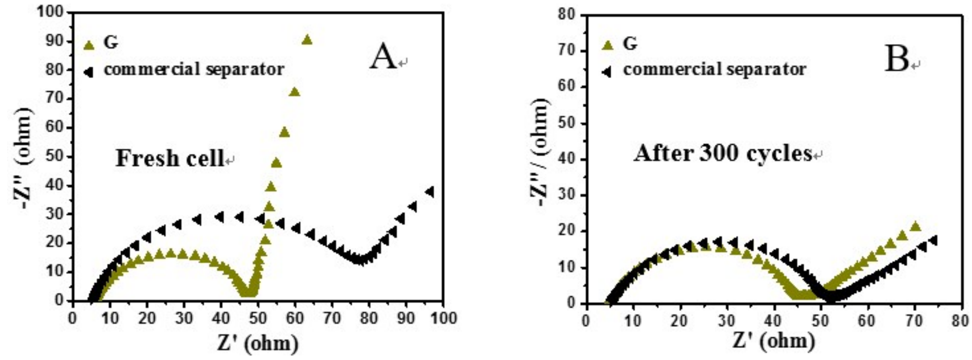

Fig. S14. Nyquist plots of cells with graphene-only coated separators (G) and commercial separator. (a) before cycling and (b) after 300 cycles at 1 C from 100 kHz to 10 mHz at room temperature.

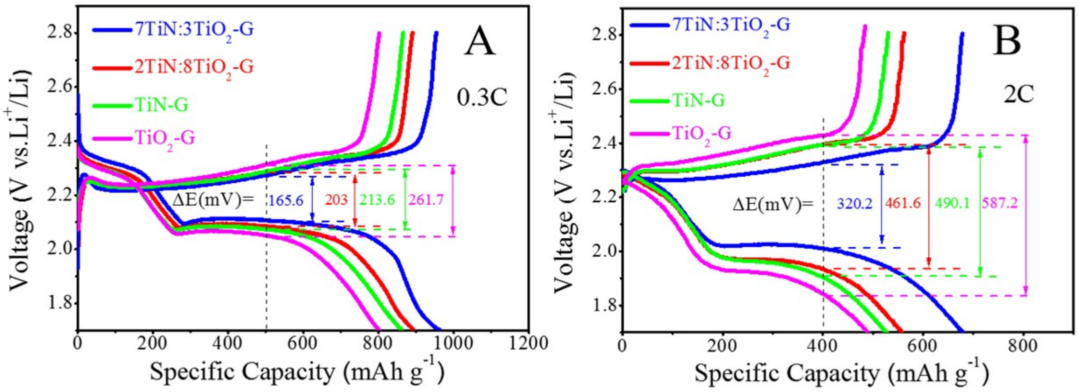

Fig. S15. Charge/discharge profiles at 0.3 C and 1 C. (a and b) The charge/discharge profiles of the cells with 7TiN:3TiO_2-G, 2TiN: 8TiO_2-G, TiN-G and TiO_2-G with the overpotentials (ΔE) labeled.

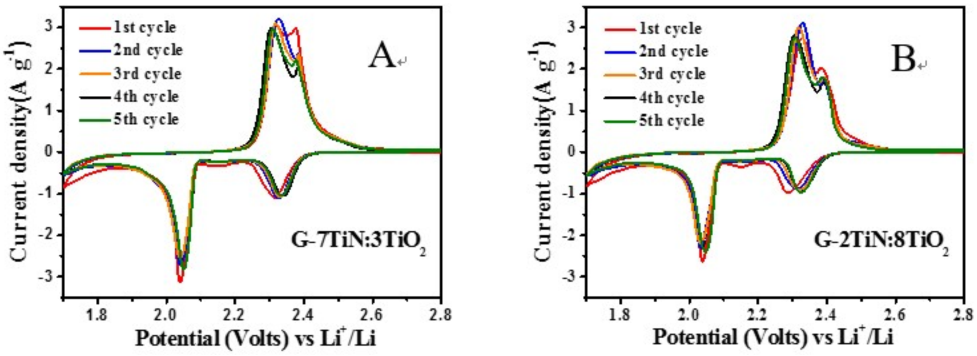

Fig. S16. Cyclic voltammograms profiles. The cells with (a) 7TiN:3TiO_2-G, (b) 2TiN: 8TiO_2-G over a voltage range from 1.7 to 2.8 V.

Table S1. Summary of performance of Li-S batteries with different interlayers or coating layers.

Sample number	Reference	Interlayer/ Coating layer	Cathode	Electrochemical performance
I	**This work**	**7TiN: 3TiO_2-G**	**Graphene/S**	**1C, 2000 cycles, 704 mAh g^{-1}, (89.1% capacity retention); 0.3C, 300 cycles, 926 mAh g^{-1} (92% capacity retention)**
Ⅱ	[1] *Nature Energy* **1**, 16094 (2016)	MOF@GO	MesoC-sulfur	1C, 1500 cycles, 855 mAh g^{-1}, (71% capacity retention)
Ⅲ	[2] *Adv Mate* **28**, 9551-9558 (2016)	LDH@NG	MWCNT-S	3.4 mAh cm^{-1}, 100 cycles, 800 mAh g^{-1}
Ⅳ	[3] *Adv Mater* **28**, 9797-9803 (2016)	black-phosphorus modified	Pure sulfur	0.4 A/g, 100 cycles, 800 mAh g^{-1}, (86% capacity retention)
Ⅴ	[4] *Adv Mater* **27**, 641-647 (2015)	Graphene	Pure sulfur	1.5A/g, 500 cycles, 663 mAh g^{-1}, (71.1% capacity retention)
Ⅵ	[5] *Nano Energy* **30**, 1-8 (2016)	G+LTO	Pure sulfur	1 C, 500 cycles, 697 mAh g^{-1}, (85.7% capacity retention)
Ⅶ	[6] *Nano Energy* **17**, 224-232 (2015).	Graphene embedded Carbon Fiber film	Pure sulfur	1 C, 300 cycles, 798 mAh g^{-1}
Ⅷ	[7] *Advanced Functional Materials* **25**, 5285-5291 (2015)	Functional Mesoporous Carbon	MesoC-sulfur	0.5 C, 500 cycles, 723 mAh g^{-1}
Ⅸ	[8] *Nano Energy* **30**, 138-145 (2016)	MPBL-coated	NPCS-S	1 C, 1000 cycles, 472 mAh g^{-1}, (57.6% capacity retention)

References

1. S. Bai, X. Liu, K. Zhu, S. Wu and H. Zhou, *Nat. Energy*, 2016, **1**, 16094.
2. H. J. Peng, Z. W. Zhang, J. Q. Huang, G. Zhang, J. Xie, W. T. Xu, J. L. Shi, X. Chen, X. B. Cheng and Q. Zhang, *Adv. Mater.*, 2016, **28**, 9551-9558.
3. J. Sun, Y. Sun, M. Pasta, G. Zhou, Y. Li, W. Liu, F. Xiong and Y. Cui, *Adv. Mater.*, 2016, **28**, 9797-9803.
4. G. Zhou, L. Li, D. W. Wang, X. Y. Shan, S. Pei, F. Li and H. M. Cheng, *Adv. Mater.*, 2015, **27**, 641-647.
5. Y. Zhao, M. Liu, W. Lv, Y.-B. He, C. Wang, Q. Yun, B. Li, F. Kang and Q.-H. Yang, *Nano Energy*, 2016, **30**, 1-8.
6. L. Chai, J. Wang, H. Wang, L. Zhang, W. Yu and L. Mai, *Nano Energy*, 2015, **17**, 224-232.
7. J. Balach, T. Jaumann, M. Klose, S. Oswald, J. Eckert and L. Giebeler, *Adv. Funct. Mater.*, 2015, **25**, 5285-5291.
8. S. Niu, W. Lv, G. Zhou, H. Shi, X. Qin, C. Zheng, T. Zhou, C. Luo, Y. Deng, B. Li, F. Kang and Q.-H. Yang, *Nano Energy*, 2016, **30**, 138-145.